C. Liauzun, D. Le Bihan, J.-M. David, D. Joly, B. Paluch
(ONERA)

E-mail: cedric.liauzun@onera.fr

DOI: 10.12762/2018.AL14-10

Study of Morphing Winglet Concepts Aimed at Improving Load Control and the Aeroelastic Behavior of Civil Transport Aircraft

Morphing is today widely studied in order to improve aircraft performance and thereby decrease their environmental footprint. This paper deals with the preliminary study of several morphing winglet concepts aimed at improving load control and aeroelastic behavior. The first step consisted in building and validating low-CPU-time-consuming but accurate aeroelastic models able to take into account aerodynamics, structural dynamics and flight mechanics, in order to handle free flexible aircraft. Aeroelastic state-space models have therefore been built from a structural modal reduction and from a rational function approximation of the aerodynamic forces based on the Roger formulation. They have been validated through comparisons with high-fidelity fluid-structure (CFD-CSM) coupling simulations. The flight mechanics has been taken into account by coupling these models with the AVL software. The second step consisted in designing a realistic reference wing equipped with a conventional winglet. Then, four morphing winglet concepts were assessed: a flapping winglet, a winglet whose deformation in torsion is controllable, a winglet able to rotate around an axis along its span and a winglet equipped with a trailing edge flap. The latter concept was found to be the most promising in terms of load control, in particular when used in conjunction with the aileron. Finally, a technological study was performed in order to ensure the feasibility of the concepts. This study was pursued up to the drawing phase, but stopped before a demonstrator was manufactured. Nevertheless, it demonstrated the feasibility of a winglet equipped with a trailing edge flap, at both the demonstrator and real aircraft scales.

Introduction

Flight transport has greatly increased over these last years, which has entailed a great number of technological developments to make aircraft increasingly larger and more performant. However, recent events, such as the increase in oil prices in 2008, or even in the '70s, and the compelling need to combat global warming led the EU to define new objectives for the aeronautic community, in order to drastically decrease the aerial transport environmental footprint (VISION2020 and FLIGHTPATH2050 [1]). In order to meet such challenges by at least reducing fuel consumption, both the aircraft structural weight and its aerodynamic performance – especially drag – must be significantly improved.

Aerodynamic performance has been greatly improved by the use of winglets. Such wingtip devices, patented for the first time by F. W. Lanchester in 1897, were developed and made popular by R. Whitcomb [29]. He showed that winglets yield better lift to drag ratios and lead to a decrease in induced drag by diminishing the trailing-edge-induced vortex intensity. They therefore enable the aircraft range to be increased. Nowadays, all aircraft manufacturers have carried out, or are currently carrying out, studies to improve this device and mount it on most aircraft (e.g., Gulfstream business jets, the Boeing blended winglet, the Airbus Sharklet, and the Spiroid winglet by Partner Aviation Inc., among others).

Another way of improving aerodynamic performance is by morphing, that is, the capability of an aircraft to adapt its geometry to the flight conditions. Two of the most famous examples are the Grumman F14 Tomcat fighter aircraft, able to change its wing sweep angle according to the flight speed, and the droop nose of the Concorde aircraft, whose fuselage nose could be deflected downwards, not to improve the aerodynamic performance, but rather to make landings possible. Discussions about the definition of "morphing" and its challenges are given in [25] and [18], and potential benefits are shown in [20]. This kind of technique, inspired by numerous examples provided by Nature (birds, fish, and insects), is not recent (see C. Ader's "Eole" aircraft built in 1890, and the Wright Brothers' wing wrapping used to control the Wright Flyer in 1903), but recent technological advances in terms of materials (composites, rubber or highly-flexible materials, and smart materials), actuators (piezoelectric, electromechanical, shape-memory alloy), sensors, computers, controllers, and computational techniques, have allowed new morphing ideas and technologies to be developed [8]. Some of them consist in modifying the upper surface, in order to delay downstream the laminar-turbulent transition location according to the flight conditions, and thereby decrease drag and fuel consumption [21], through changing the wing trailing edge camber using a three-hinge device to improve the lift-over-drag ratio, or drag [19]. This is, of course, far from being exhaustive and a review of morphing technologies can be found in [5]. A recent overview of what morphing implies for aeronautics can be found in [9].

Both previous ways of decreasing drag and weight have also been combined. Several morphing winglet concepts have indeed been patented [23] [6] [26], or have been studied or assessed. Different kinds of morphing have been considered. Control surfaces at the leading or/and trailing edges have been added to the winglet to control vortices under high-lift conditions [3], or to improve the lift-to-drag ratio and the gust-load alleviation [28]. A winglet with a trailing edge flap has been designed and assessed in terms of both aerodynamic performance and loads, taking into account the certification requirements within the framework of the European Union project SARISTU [27] [17]. Another morphing winglet based on a chiral-type internal structure has been designed, enabling cant, twist and camber control throughout the flight envelope [10].

The main motivation for developing morphing winglet concepts is, most often, to improve the aerodynamic performance. The goal of this study is to assess the potentiality of such a device to improve load alleviation, and therefore the aircraft aeroelastic behavior.

The first part of the paper gives a brief description of the four morphing winglet concepts that are assessed. The second part, dedicated to the aeroelastic models used for the evaluation, presents the theoretical aspect, the preliminary results and their validation by comparisons with CFD simulations. The third part is devoted to the evaluation of the concepts, used alone or in combination with a conventional aileron. The last part focuses on the technological point of view to demonstrate the feasibility of the most promising concept.

Morphing Winglet Concepts

The main idea consists in adding a new control surface on the winglet, or making it moveable, in order to improve load control. The latter is assessed as the capability to decrease the wing root bending moment in cases where critical and sizing loads are applied. This bending moment decrease would thus allow the structure weight to be reduced. Several concepts are evaluated with that goal, as well as with the constraint of not altering drag (Figure 1). The first concept consists in applying torsion around an axis along the winglet span, and then driving the toe angle and modifying the apparent incidence. Such a morphing shape can be achieved by replacing winglet ribs with actuators to drive the position of the spars relative to one another thereby creating a kind of shear deformation of the sections. The second concept can be seen as a limit case of the previous one, and consists of a rotation of the whole winglet around a span-wise axis. The third one is a kind of flapping, thereby allowing the cant angle to be driven. The last concept considers a trailing edge equipped with a single-hinged flap.

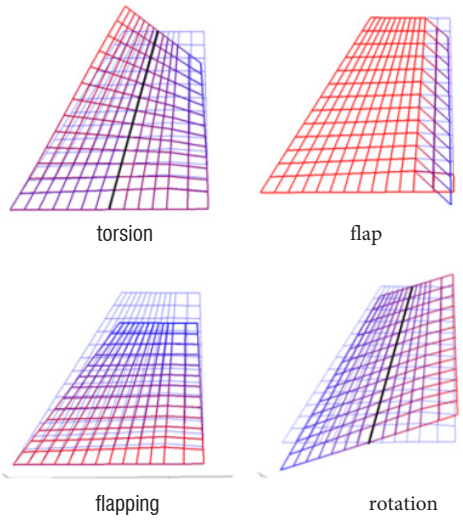

Figure 1 – Morphing winglet concepts

These morphing concepts are evaluated for a transport aircraft whose top level requirements and wing geometry were provided by Alenia within the framework of the European project SARISTU [30]:

- Npax: 130
- Range: 3,000 NM
- MTOW (Maximum Take Off Weight) = 60,000 kg
- MLW (Maximum Landing Weight) = 55,000 kg
- Design cruise speed = Mach 0.75 at 35,000 ft

The geometrical characteristics are:

- Reference surface = 111 m^2
- Span = 34.14 m
- Dihedral angle = 3.5°
- Sweep angle at the leading edge = 18°
- Mean aerodynamic chord = 3.7457 m

The efficiency of these concepts is evaluated for cruise flight conditions.

Aeroelastic Models

Aeroelastic Reduced Model

The winglet concept efficiency is assessed using a reduced aeroelastic model aimed at computing loads, the global aerodynamic lift coefficient, aerodynamic forces and structural deformations. The model is based on a fluid-structure state-space model. It is built, on the

one hand, from a structural model classically projected onto a modal basis to compute the dynamic behavior and, on the other hand, from a reduced aerodynamic model to obtain the aerodynamic forces.

The main advantage of state-space models lies in their simplicity, since they are able to provide any physical quantity (displacements, forces, moments, twist angle, etc.) from linear relations. They are also very useful and convenient for the control-surface controller law determination. The state-space model is indeed expressed in the time domain as

$$\begin{cases} E\dot{x}(t) &= Ax(t)+Bu(t) \\ y(t) &= Cx(t)+Du(t) \end{cases} \quad (1)$$

where x is the state vector, y is the vector of quantities of interest and u is the command (input) vector. u is, in the case of morphing winglet evaluation, the vector of the control-surface deflections. It can also be a turbulence perturbation in the case of load alleviation assessment, or rigid mode coordinates in the case of flight mechanics. E, A, B, C and D are matrices that are independent of time, x and u, but can depend on other parameters (e.g., flight characteristics, such as the flight speed V and the air density ρ). In the case of aeroelastic models, these matrices are built from structural mass, damping and stiffness matrices, or their projection onto a modal basis. The structural model is enriched with the aerodynamic force representation resulting from a Rational Function Approximation (RFA) model [24]. Such a model assumes that the aerodynamic forces are proportional to the structural motion and that the proportionality coefficient, also called the Aerodynamic Influence Coefficient (matrix $\frac{1}{2}\rho V^2 A$), can be written in the Laplace domain, with s being the Laplace variable, as

$$A(s) = D_0 + D_1 s + D_2 s^2 + \sum_{i=1}^{n_a} E_{i+2}\frac{s}{s-\lambda_i} \quad (2)$$

where D_0 D_1 and D_2 denote the aerodynamic stiffness damping and inertia, and n_a is the number of aerodynamic states. The denominator zeros λ_i are the lag coefficients. With each lag term or partial fraction can be associated an aerodynamic state η_i defined as

$$\eta_i = s\left[(s-\lambda_i)I\right]^{-1} E_{i+2}x$$

The latter relation can be expressed in the time domain as

$$\dot{\eta}_i = E_{i+2}\dot{x} + \lambda_i \eta_i$$

The RFA model then allows an aeroelastic state-space model to be built. If the structure mass, damping and stiffness are modeled by the matrices M, C and K, the aeroelastic model can be written as

$$\partial_t \begin{pmatrix} x \\ \dot{x} \\ \eta \end{pmatrix} = \begin{bmatrix} I & 0 & 0 \\ 0 & M-\frac{1}{2}\rho V^2 D_2 & 0 \\ 0 & 0 & I \end{bmatrix}^{-1} \begin{bmatrix} 0 & I & 0 \\ -\left(K-\frac{1}{2}\rho V^2 D_0\right) & -\left(C-\frac{1}{2}\rho V^2 D_1\right) & \frac{1}{2}\rho V^2 \begin{bmatrix} I & \cdots & I \end{bmatrix} \\ \begin{bmatrix} 0 \\ \vdots \\ 0 \end{bmatrix} & \begin{bmatrix} E_3 \\ \vdots \\ E_{n_a+2} \end{bmatrix} & \begin{bmatrix} \lambda_1 I & \cdots & 0 \\ \vdots & \ddots & \vdots \\ 0 & \cdots & \lambda_{n_a} I \end{bmatrix} \end{bmatrix} \begin{pmatrix} x \\ \dot{x} \\ \eta \end{pmatrix} \quad (3)$$

The RFA model used for the assessment of the morphing winglet was that proposed by Roger [22]. In order to reduce the number of states, the structure is usually projected onto a rather small -eigen-mode basis. The number of aerodynamic states is then equal to the number of these structure modes times a number of lag terms (n_L), which has to be determined as a compromise between the requirement of a small number of total states and an accurate approximation of the Generalized Aerodynamic Forces (GAF, aerodynamic forces projected onto the structural modes). Computation of the RFA matrices is performed in such a way that the best approximations of tabulated known GAF data are determined using a least square algorithm. These tabulated data are obtained using an unsteady aerodynamic code able to compute the aerodynamic pressure or force variation due to a purely oscillatory motion at prescribed frequencies. The lag coefficients are determined from an optimization process aimed at minimizing the angular variation between the aerodynamic force components (GAF_{ij}) resulting from the RFA model and from the tabulated data.

$$\min\left[1-\frac{\left(\mathrm{GAF}_{ij}^{\mathrm{RFA}},\mathrm{GAF}_{ij}^{\mathrm{tab}}\right)^2}{\left\|\mathrm{GAF}_{ij}^{\mathrm{RFA}}\right\|^2\left\|\mathrm{GAF}_{ij}^{\mathrm{tab}}\right\|^2}\right]$$

The evolutions of the damping and frequencies resulting from the state-space model are strongly dependent on this GAF smoothing process. That is why the optimization process has to be carried out taking into account the following parameters: number of tabulated frequencies to be able to catch the GAF loop-like evolutions in the complex plane, the number (n_L) and type of the lag coefficients (real or imaginary), and the range within which they are selected. A first guess of the latter parameter is given by a flutter analysis using the classical double scanning p-k method and only the tabulated GAF.

The system (3) represents the first equation of the aeroelastic state-space model (1) and can be enriched by an observation equation expressing the expected quantity (bending moment, lift coefficient, displacement, etc.) as a function of the unknown states, thus representing the second equation of (1). Nevertheless, if the structure is modelled by a modal representation, the state-space model is used to compute the deformation of the wing. The latter deformation is then transferred (through interpolation or smoothing) to the aerodynamic grid, thereby updating the geometry, which can be used as input for a fast aerodynamic code to provide integrated forces, such as the lift force or the bending moment at the wing root. Another way to compute them consists in calculating the integrated forces for each mode using the aerodynamics code and in combining them linearly with the generalized coordinates as coefficients.

First Evaluation of the Concepts

In a first step, a preliminary finite-element model of a wing with a conventional winglet has been built, taking into account classical wing

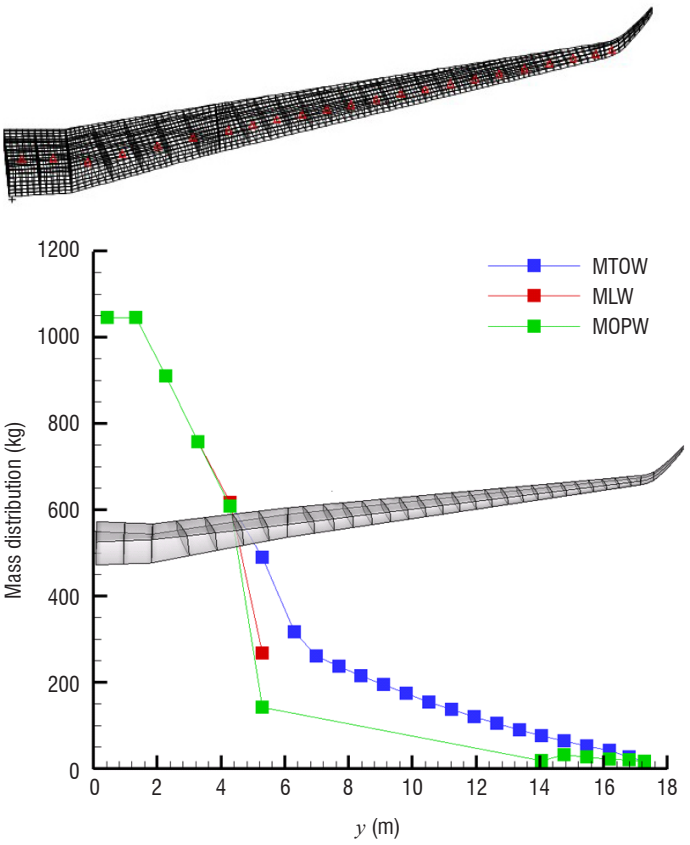

Figure 2 – Wing preliminary finite-element model and fuel mass distribution along span

architecture (spars, ribs, stringers, mass penalty for the leading edge trailing edge and equipment) and primary structures (spars, ribs, stringers and skin). The model is made out of a composite material and has been sized according to two symmetric load cases with load factors equal to 2.5 and –1. It has been validated with respect to flutter and buckling. Kerosene has been added to this model as one-node elements connected to the wing box with rigid elements, according to the distribution shown in Figure 2. Furthermore, the winglet has been modeled as a continuity of the wing and not as a separate device that can be plugged into it.

In the second step, aimed at morphing winglet concept assessment, an aeroelastic state-space model has been built from first structural elastic modes, rigid modes, control surface commands (winglet concepts, aileron and inner flap) and generalized aerodynamic forces (GAF), whose dependency on the frequency is computed using the Roger formulation [22] described above. The tabulated aerodynamic forces used as input for the Roger model are computed at some oscillation frequencies using the Doublet Lattice Method (DLM) [2], which is based on the assumption of linear subsonic aerodynamics. This panel method actually computes the local unsteady pressure variations and then the force variations due to a harmonic motion at a given frequency. This motion can be due to rigid modes, elastic deformation modes of the wing or a rotation of a control surface. Since DLM is a linear formulation, those variations are, in fact, the derivatives of the pressure or forces (after integration) with respect to the lifting surface motion.

Such a model has been built from the first seven structural elastic deformation modes of the preliminary finite-element model (Figure 3), from the control surface command highlighted in light blue (winglet)

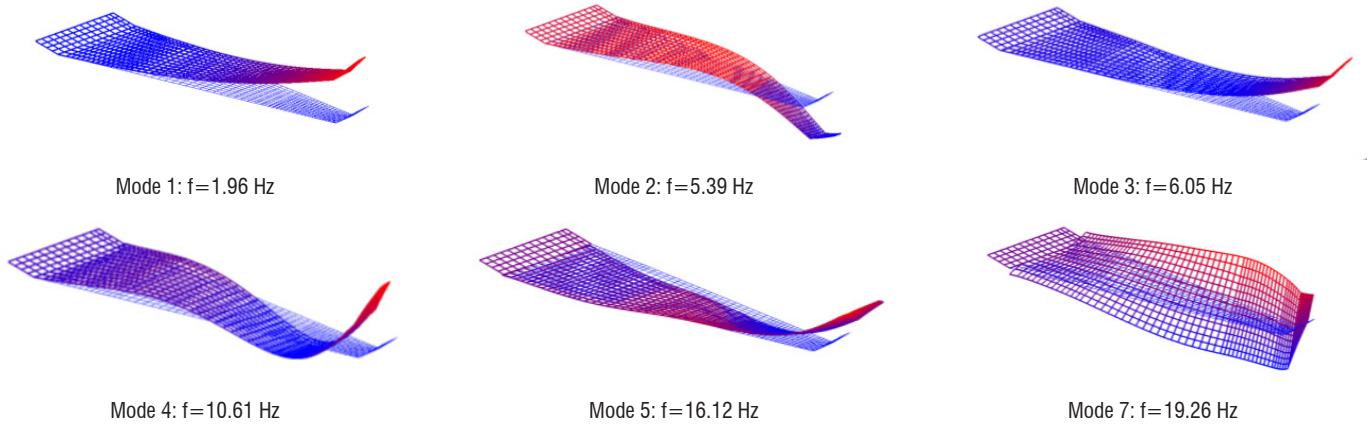

Figure 3 – Structural eigen-modes of the wing preliminary finite-element model (clamped root)

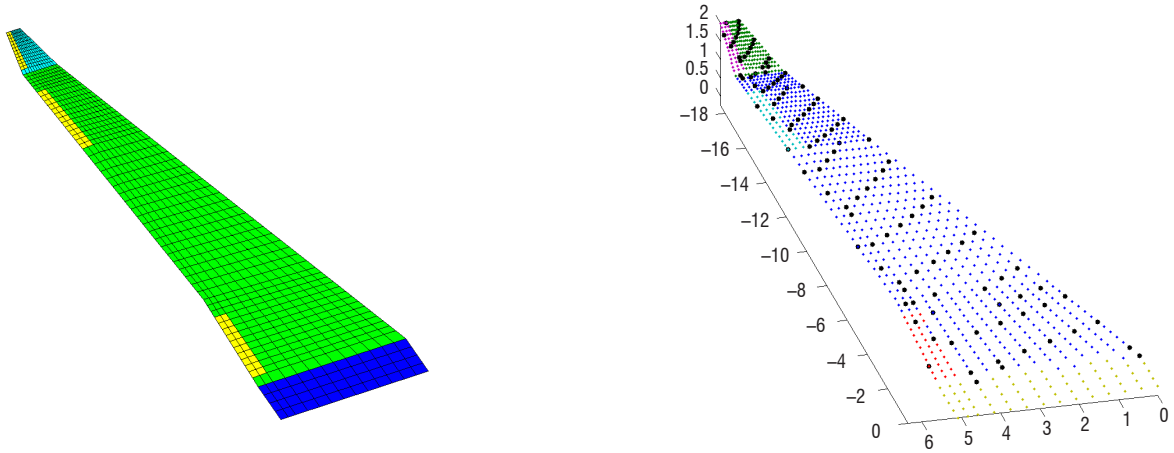

Figure 4 – Panel mesh for aeroelastic force calculation using DLM (left) and measurement locations (right) for the state-space model

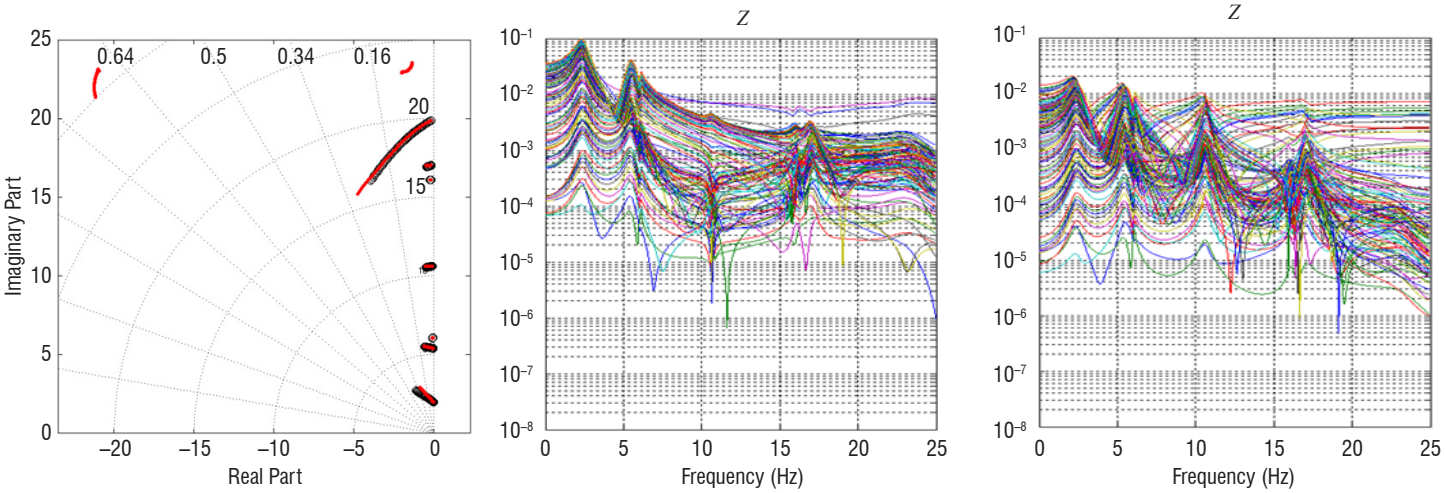

Figure 5 – Eigen-values of the aeroelastic system resulting from both the state-space model and a classical flutter analysis using a p-k method (left); displacement FRF due to the aileron deflection (middle) and to the deflection of the deformable-in-torsion winglet (right)

and yellow (aileron, inner flap and winglet flap) in Figure 4, from the plunge and pitch flight mechanics modes, and from a cylindrical turbulence mode. The aerodynamic computations providing the tabulated GAF used to build the RFA model have been performed at the cruise Mach number.

The GAF smoothing has been validated by comparing the evolution of the fluid-structure system complex eigen-values resulting from the state-space model and from a flutter analysis using the p-k method (Figure 5 left). Figure 5, middle and right, show the vertical displacement FRF of all observation points (Figure 4 right) in response to the aileron (middle) and to the deformable-in-torsion winglet (right) deflections. A displacement 5 times greater can be noticed when the aileron is deflected.

In a third step, every winglet concept has been assessed using this reduced aeroelastic model. Table 1 gives the vertical force variation at the wing root resulting from the different input commands at null frequency (quasi-static computations): pitching flight mechanics mode, turbulence, wing internal flap deflection, aileron deflection, rotation of the whole winglet around an axis along its span, torsionally-deformable winglet deflection, and winglet trailing-edge-flap deflection. As expected at the cruise Mach number, the effectiveness loss due to the structural flexibility is higher for the winglet and aileron commands. Furthermore, the impacts on the vertical effort of the torsional winglet and of the winglet flap are significantly higher than the impacts of

	pitching motion	turbulence	internal flap	aileron	winglet rotation	torsional winglet	winglet TE flap
rigid wing	120102	125994	–9693	–7930	73	839	–1033
flexible wing	110420	118178	–8818	–3265	–4	284	–139
ratio (%)	8	6	9	59	105	72	86

Table 1 – Vertical effort variation (in Newton) at the wing root for 7 input static commands

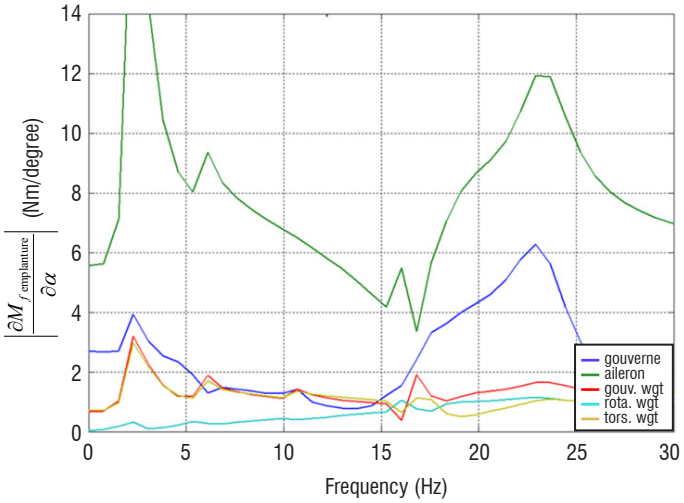

Figure 6 – Bending moment variation at the wing root for the deflection of the internal flap (blue curve), aileron (green), winglet TE flap (red), whole winglet (rotation) (light blue) and torsional winglet (yellow)

the other morphing winglet concepts. The wing root bending moment variation for non-zero frequencies has also been investigated, taking into account the structure flexibility (Figure 6). The effectiveness of the aileron is significantly higher than that of the other commands for the entire frequency range considered. The morphing winglet concepts, like the aileron, are most efficient at a frequency matching the first structural bending eigen-frequency.

Comparisons with High-Fidelity Fluid-Structure Coupling Simulations

The previous aeroelastic model has been built from a DLM formulation for the aerodynamic forces, which does not take into account either the fluid viscosity or the flow discontinuities like shocks or flow separation. In order to validate the latter model, high-fidelity fluid-structure coupling simulations have been carried out for both the deformable-in-torsion and the trailing-edge-flap winglet concepts. Such simulations model the fluid behavior with RANS CFD and the structure with the preliminary finite-element model. They have indeed been performed using the in-house CFD software

elsA [7] [14] associated with the aeroelastic module Ael [15] [16] for the two winglet concepts, as well as for the aileron (Figure 7). The control-surface static deflections have been carried out by mesh deformation, as can be seen in Figure 8. The control-surface effectiveness has been computed for cruise conditions (Mach=0.75, C_L=0.52, altitude=35,000 ft).

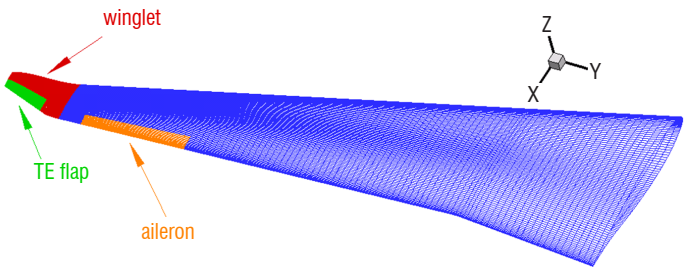

Figure 7 – Wing surface CFD mesh with the movable surfaces in orange, red and green

Such fluid-structure coupling simulations, like the ones using the reduced aeroelastic model, allow the impact of a control surface deflection on the aerodynamic performance to be investigated, as well as the impact on the aeroelastic wing deformations and on load alleviation. The efficiency loss due to the structural flexibility of the wing can also be assessed by comparing simulations carried out with a flexible structure (fluid-structure coupling simulations, named "AEL" in the following figures) and with an infinitely rigid wing (only fluid computations named "CFD" in the figures). First of all, the behavior of all control surfaces remains linear throughout the entire deflection range, except for the winglet trailing-edge-flap, whose linearity deflection range goes up to 5°. This checks that the case of this wing under the considered cruise flight conditions is within the validity range of the DLM formulation. From the aerodynamic performance point of view, unlike the aileron, a positive (downwards) or negative (upwards) deflection of the whole winglet, or of the winglet trailing edge flap, yields a drag increase (Figure 9 middle). This is indeed expected, since the simulations have been performed for cruise conditions, for which the shape of the transport aircraft wing and winglet is optimized. Nevertheless, the lift-over-drag ratio can be slightly increased, which shows the great potentiality of morphing winglet to improve the performance during at least the whole cruise. The second point is that an important loss of control-surface effectiveness (defined as the lift variation over the deflection variation, or as the slope of the lift evolution with respect to the deflection angle, Figure 9 left) due to the structural flexibility can be noticed, except for the torsionally-deformable winglet (Table 2).

Control surface	Rigid effectiveness (/°)	Flexible effectiveness (/°)	Effectiveness loss (%)
aileron	0.0063	0.0034	46
torsional winglet	0.0005	0.000375	25
winglet TE flap	0.0016	0.00073	54

Table 2 – Effectiveness of three control surfaces: aileron, deformable-in-torsion winglet and winglet trailing edge flap

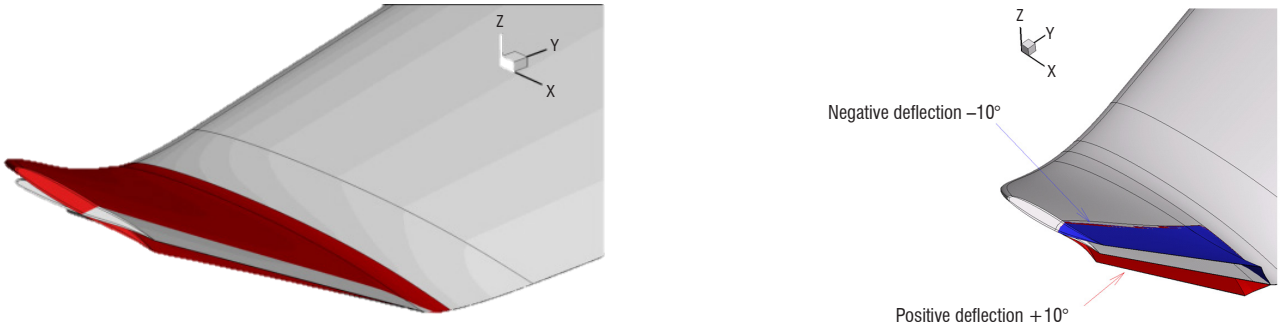

Figure 8 – CFD mesh surfaces on winglet: deformable-in-torsion winglet on the left, and trailing-edge-flap on the right

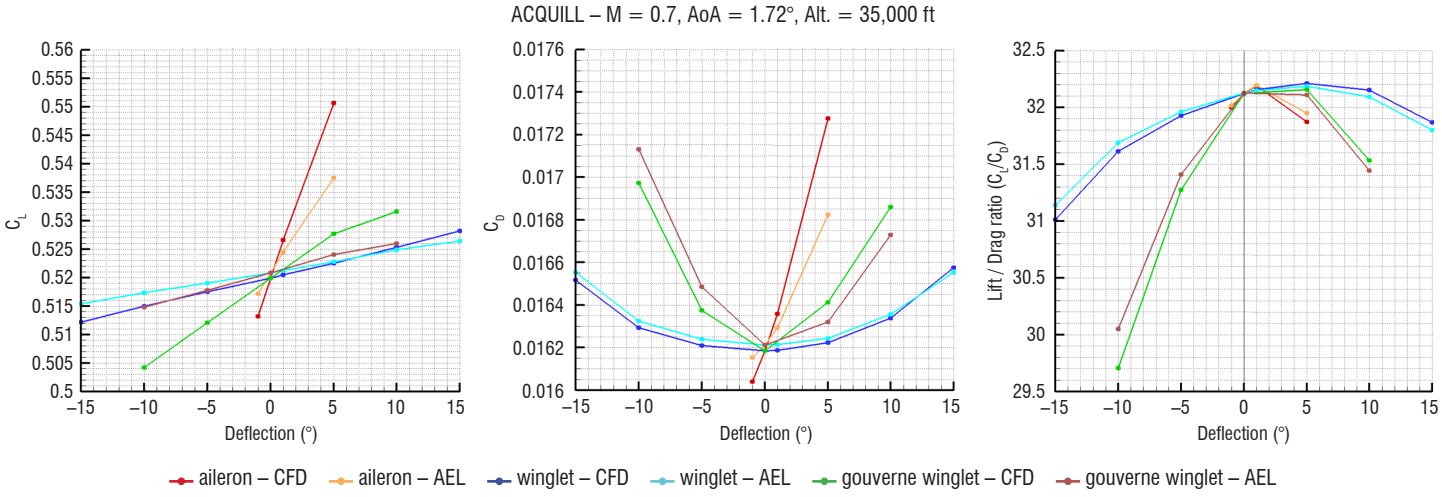

Figure 9 – Lift, drag and lift-over-drag evolution with respect to the control surface (aileron, deformable-in-torsion winglet and winglet TE flap) deflection

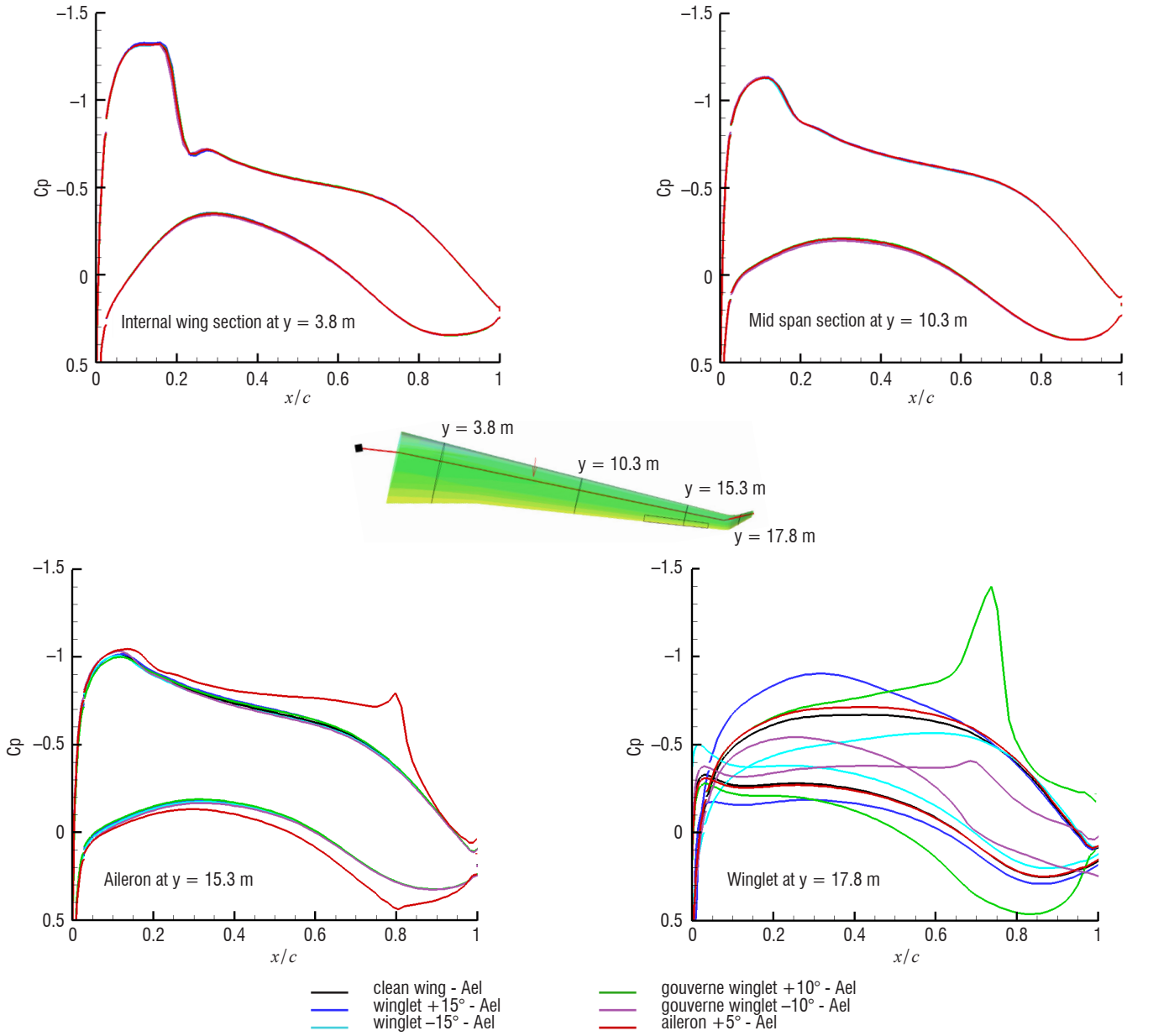

Figure 10 – Pressure distributions on 4 wing sections

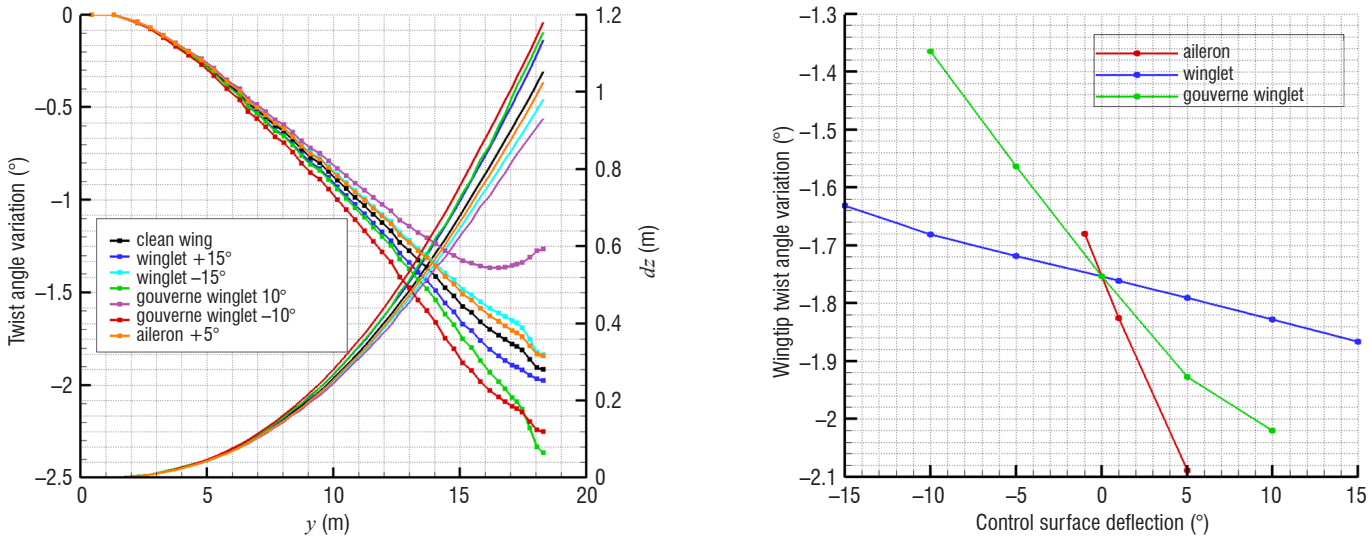

Figure 11 – Aeroelastic deformations due to control surface deflection (aileron: red and orange curves, torsional winglet: blue and cyan curve, winglet TE flap: green and purple curves) with respect to the span coordinate (left) and deflection angle (right)

From an aeroelastic point of view, Figure 11 shows the aeroelastic deformations (twist angle variation and vertical displacements along the span) of the wing thanks to aileron and morphing winglet deflections. The figure also shows (plot on the right) the twist angle of the wing tip with respect to the deflection of the three control surfaces. Even if the pressure perturbations due to the deflection remain local (see Figure 10), particularly if the control surface is the winglet itself or its flap, the impact of the deflection on the twist angle variation along the span is significant for both the aileron and the winglet trailing edge flap.

In terms of loads, the impact of morphing winglet deflections can be seen in Figure 12. The middle and right-side plots indeed show the span-wise distribution of the local bending moment induced by the pressure integration along the only chord for fixed sections. The plot on the left represents the span evolution of the bending moment integrated along the span.

The reduced aeroelastic model and the high-fidelity fluid-structure coupling modelling were then compared. A good agreement was noticed with regard to the qualitative behavior of the control surfaces in terms of aerodynamic load alleviations, even though the levels are slightly different, as can be seen in Table 3.

	$\Delta C_L / °$	
control surface	*elsA*-Ael	state-space model
aileron	0.0034	0.0025
torsional winglet	0.0004	0.00025

Table 3 – Lift variation induced by aileron or torsional-winglet deflection

Morphing Winglet Concept Evaluation

Design of a Realistic Reference Wing

CFD computations have shown the validity of the reduced aeroelastic models based on a state-space formulation for the aerodynamic conditions of interest in this study. In order to assess the innovative morphing concepts, such reduced models have to be built from a structural model of a wing, which should be the most representative possible of a real wing, at least from a structural point of view. The latter wing is called a "reference wing" in the following and has been designed by optimizing the preliminary finite-element model using the solvers SOL200 (optimization solver) and SOL144 (static aeroelastic solver) of the MSC/NASTRAN software, and taking into

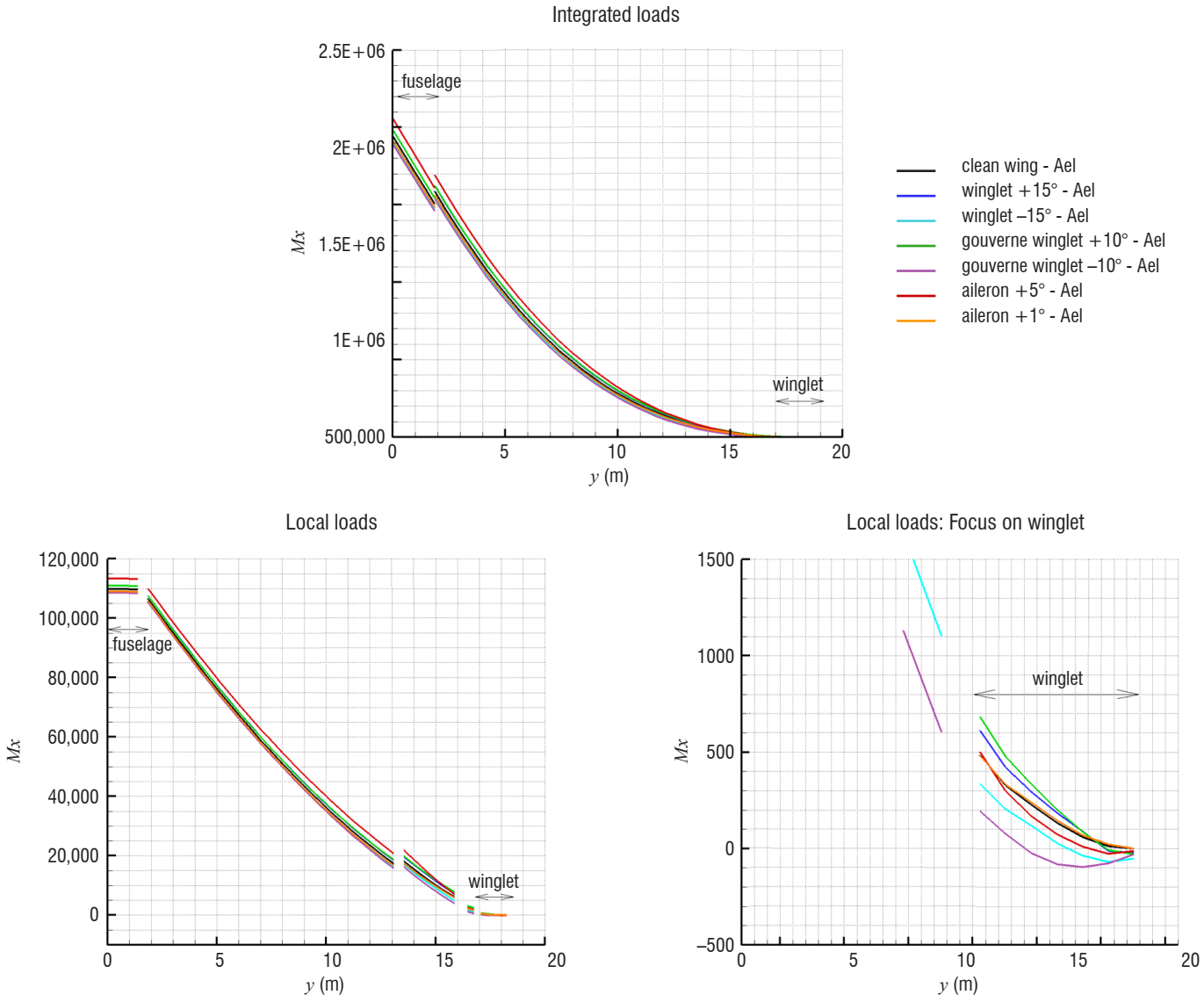

Figure 12 – Bending moment distributions along span

account both symmetric (2.5 g pull-up maneuver, gust load) and antisymmetric load cases (roll maneuver) resulting from balanced maneuvers. Aerodynamic loads have been computed using fluid-structure coupling simulations with a full free-free aircraft model. The fuselage and tail have been considered as rigid and the aircraft mass and inertia have been represented by a one-node element (CONM2) at the center of gravity of the aircraft (Figure 13 left). The optimization has been performed considering as design parameters the thickness of the skin spars and ribs of the wing box, taking into account the constraints of 3.2×10^{-3} maximal deformations in the composite shells (Figure 13 right).

Flutter stability has been checked for several flight speeds and mass configurations (MTOW, MLW and one intermediate configuration for which fuel mass is concentrated in the outer wing, which is a configuration named MOPW, see Figure 2). The resulting optimized wing is then realistic and will be used as reference for morphing winglet concept evaluations.

Morphing Winglet Assessment Based on the Reference Wing

The evaluation of the morphing winglet concepts has been performed taking into account the whole free-free aircraft described in the previous section, equipped with the optimized reference wing. Two mass configurations have been considered: MTOW (60 tons) and the intermediate configuration (called MOPW), for which fuel mass is mainly located in the fuselage and in the outer wing (Figure 2).

Two reduced aeroelastic models were then built from the first eight deformation eigen-modes, a pitching rigid mode and a "phugoid" mode (combination of plunge and pitch), a cylindrical turbulence mode, a GAF model built using a Roger approach and six control-surface deflections: deformable-in-torsion winglets, rigid rotation of the winglets, winglets with trailing edge flaps, winglets flapping, ailerons and horizontal tail planes (HTP). In order to be able to design controllers and to synthetize control laws, the number of states have been reduced to 78 using a robust algorithm available with control toolboxes (Robust Control Toolbox working with Matlab).

The latter aeroelastic models allow the effectiveness of the six control surfaces to be assessed in terms of lift variations. These effectiveness data are given for both mass configurations in Table 4. One can note that the impact of the structure flexibility on the lift variation is high for the MOPW configuration, especially for the morphing winglet concepts. This discrepancy is significantly less for the MTOW configuration, thus showing a high influence of the mass distribution on the control surface effectiveness. Moreover, and as expected from the results of the computations with the preliminary finite-element model

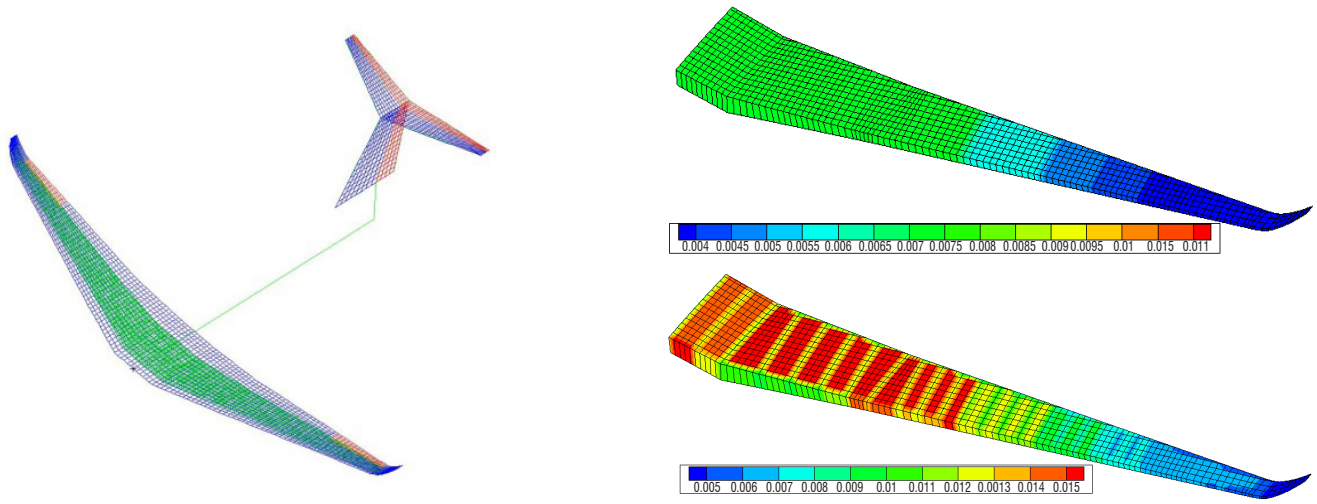

Figure 13 – Whole aircraft aeroelastic model (structure finite elements in green, aerodynamic panels in blue and control-surface aerodynamic panels in red), and shell-thickness distributions before (top right) and after (bottom right) optimization

Command	MOPW			MTOW		
	Rigid/flexible	$\partial Cz/\partial\alpha$ (/deg)		Rigid/flexible	$\partial Cz/\partial\alpha$ (/deg)	
		Rigid	Flexible		Rigid	Flexible
Torsional winglet	2.22	1.42e–04	6.41e–05	1.44	1.42e–04	9.89e–05
Aileron	1.59	2.36e–03	1.48e–03	1.25	2.36e–03	1.89e–03
Winglet flap	2.22	3.02e–04	1.36e–04	1.44	3.02e–04	2.10e–04
Winglet flapping	2.10	–2.14e–05	–1.02e–05	1.41	–2.14e–05	–1.51e–05
Winglet rigid rotation	2.12	–5.98e–04	–2.83e–04	1.41	–5.98e–04	–4.24e–04
HTP	0.98	5.01e–03	5.13e–03	0.98	5.01e–03	5.14e–03
Pitch	1.12	1.13e–01	1.01e–01	1.05	1.13e–01	1.07e–01
Phugoid	1.03	1.13e–01	1.09e–01	1.01	1.13e–01	1.11e–01
Turbulence	1.03	1.13e–01	1.09e–01	1.01	1.13e–01	1.11e–01

Table 4 – Impact of commands on lift (frequency = 0Hz)

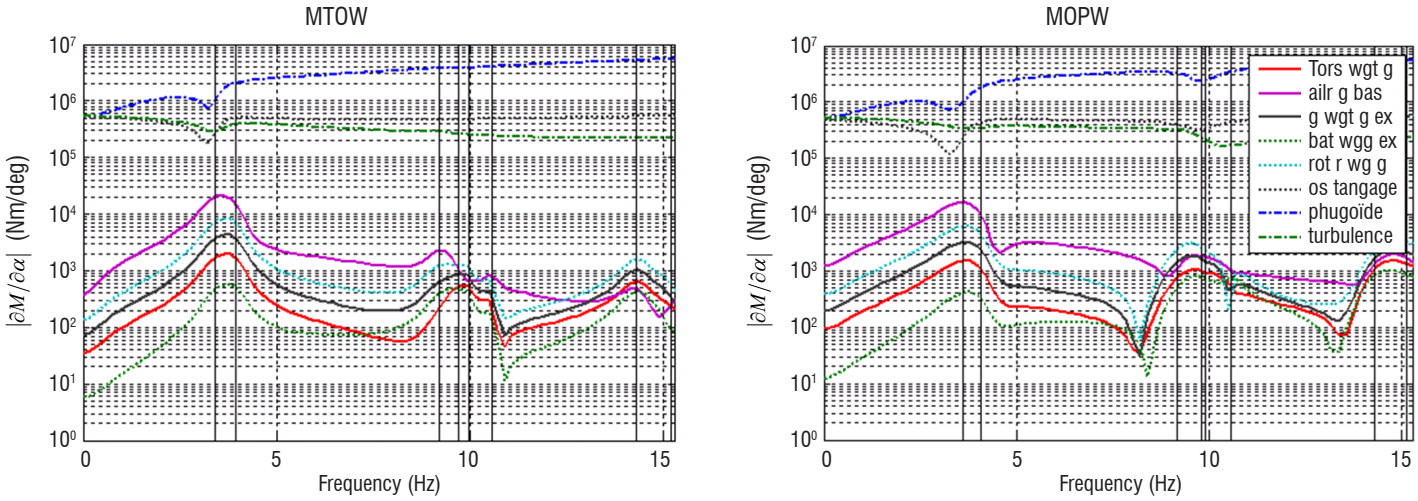

Figure 14 – Bending moment variations at the wing root vs. frequency response to the commands: winglet flapping (dotted green curve), torsional winglet (red curve), winglet flap (black curve), winglet rigid rotation (cyan curve), aileron (purple curve), turbulence (green dashed-dotted curve), pitching motion (gray dotted curve) and phugoid (dashed-dotted dark blue curve)

and using both reduced and high-fidelity fluid-structure models, one can note the greater effectiveness of the winglet flap compared to that of the torsional winglet. Furthermore, the structure flexibility induces an increase in the moment variations for all commands when their frequency is close to the structural eigen-frequencies. Similar conclusions can be drawn for the bending moment variations at the wing root (Figure 14).

The four morphing winglets presented in Figure 1 have thus been assessed in terms of variations of lift and bending moment at the root. The effectiveness of the flapping winglet has been found to be significantly lower than that of the other control surfaces. The previous simulations have also shown a lower effectiveness of the torsional winglet than that of the winglet equipped with a flap and, of course, of the aileron (Table 4 and Figure 14). This can be partly explained by geometric considerations. Taking indeed into account the surfaces of the control surfaces and their projection onto a horizontal plane, the effective surface of the torsional winglet is decreased due to its cant angle of about 50° compared to a horizontal aileron. Furthermore, the deflection of the torsional winglet is, for technological reasons, progressive according to a quadratic function ranging from 0° at the root to the wanted deflection at the tip. At last, the chord decreases also along the span to reach its minimum when the maximal deflection is applied. Those three factors lead to a loss of 2/3 of the initial surface and finally to an effective surface of 1/4 of the aileron surface.

The rotation of the winglet around an axis along the winglet span is a concept that would yield a too high mass penalty to be considered as feasible from the technological point of view. However, it can be considered as a limit case of the torsional winglet, thus allowing the highest potential of such a morphing concept to be evaluated.

Strategy of the Command of the Winglet with Flap Combined with the Aileron

The winglet with a trailing edge flap seems to be the most efficient in terms of load control from the previous evaluations. It has therefore been further investigated by assessing its load alleviation capabilities, taking into account a trimmed aircraft in flight. The reduced aeroelastic model built as described above is not able to compute the trim parameters. It has therefore been coupled with the AVL software developed by M. Drela and H. Youngren [13]. This code, based on a Vortex Lattice Method to compute aerodynamic forces, is able to compute the trim parameters (incidence, and control-surface deflection angle) for balanced static maneuvers of a rigid aircraft. Furthermore, it also computes drag, using the Trefftz formulation [4] and lift taking into account the mean chord curvature, thus allowing the evaluation of the lift at null incidence. The coupling with the reduced aeroelastic model leads then to the trim computation of a flexible aircraft. It is performed using a classic iterative method:

- Trim computation using AVL, whose outputs are the incidence, HTP deflection angle, pressure distribution on the wing surfaces and integrated pressure forces and moments at the wing root.
- Transfer of the pressure distribution onto the DLM mesh used to build the state-space aeroelastic model, and computation of the resulting generalized aerodynamic forces.
- Computation of the wing deformations using the aeroelastic state-space model.
- Translation of these deformations into AVL inputs. The vertical displacements and rotation of the mean chord of some wing sections are indeed deduced from the wing deformation.
- If no convergence is achieved, return to Step 1.

This coupling procedure has been applied to the aircraft for cruise flight conditions (load factor $n_z = 1$), in order to investigate the effect of both aileron and winglet flap deflections. The trim has been computed taking into account plunge and pitch rigid motions. Convergence has been reached after 7 iterations for every aileron and winglet flap deflection configuration, as can be seen in Figure 15, which represents the evolution of four quantities: trim parameters, *i.e.*, incidence and HTP control-surface deflection (top left), drag representing the aerodynamic performance and computed using the Trefftz formulation (top right), the bending moment at the wing root (bottom left) and a combination of both the load and aerodynamic performance (bottom right), which is a quantity that can be used for

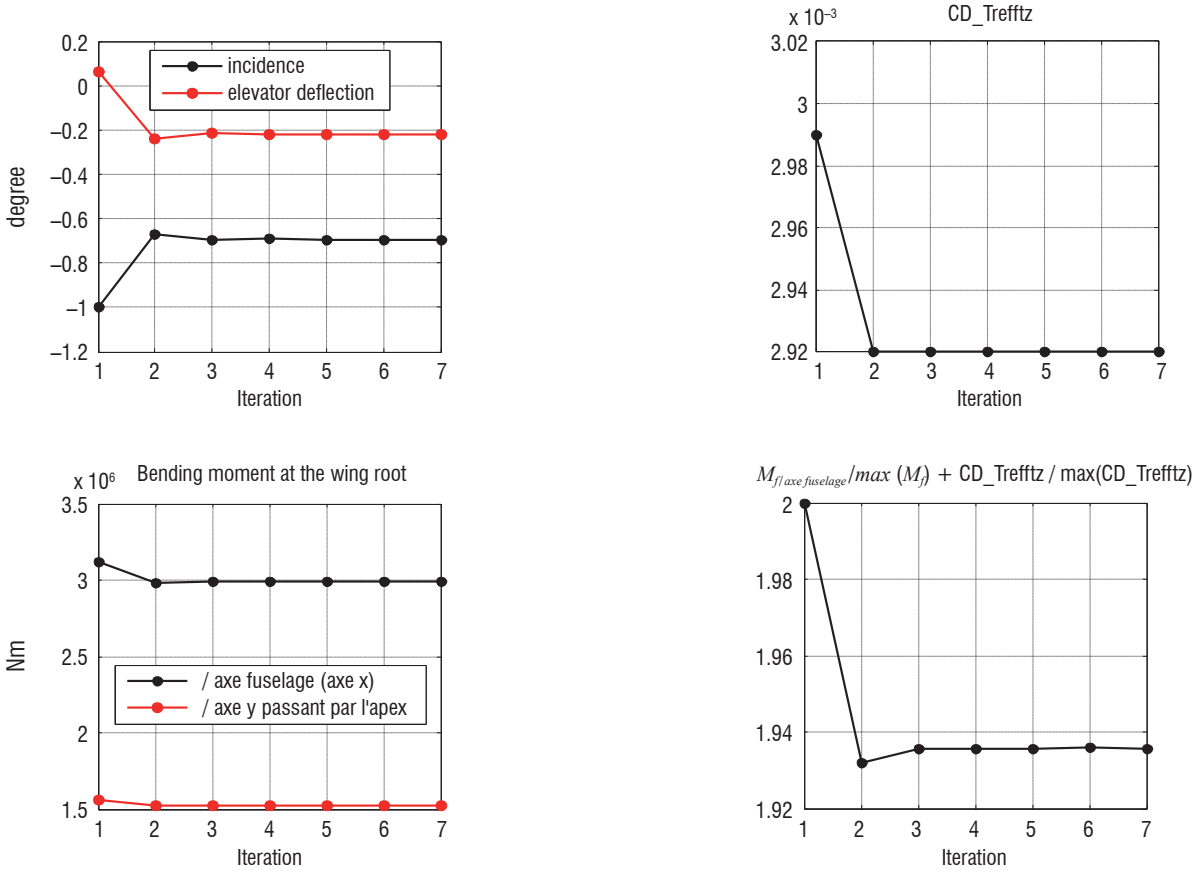

Figure 15 – Flight mechanics – elasticity coupling convergence

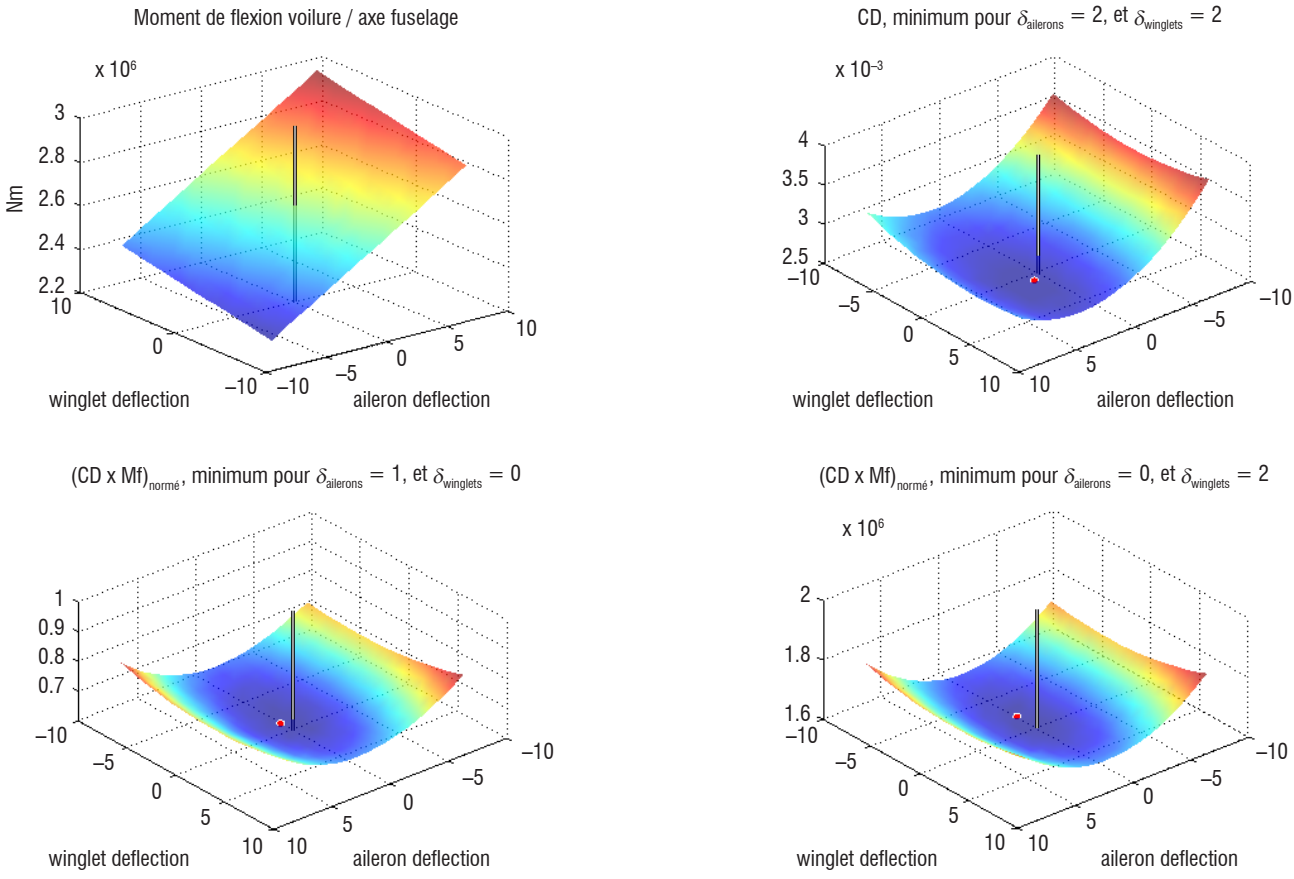

Figure 16 – Bending moment at the root (top left), drag (top right), and the product (bottom left) and sum (bottom right) of both for several aileron-winglet flap deflection configurations.

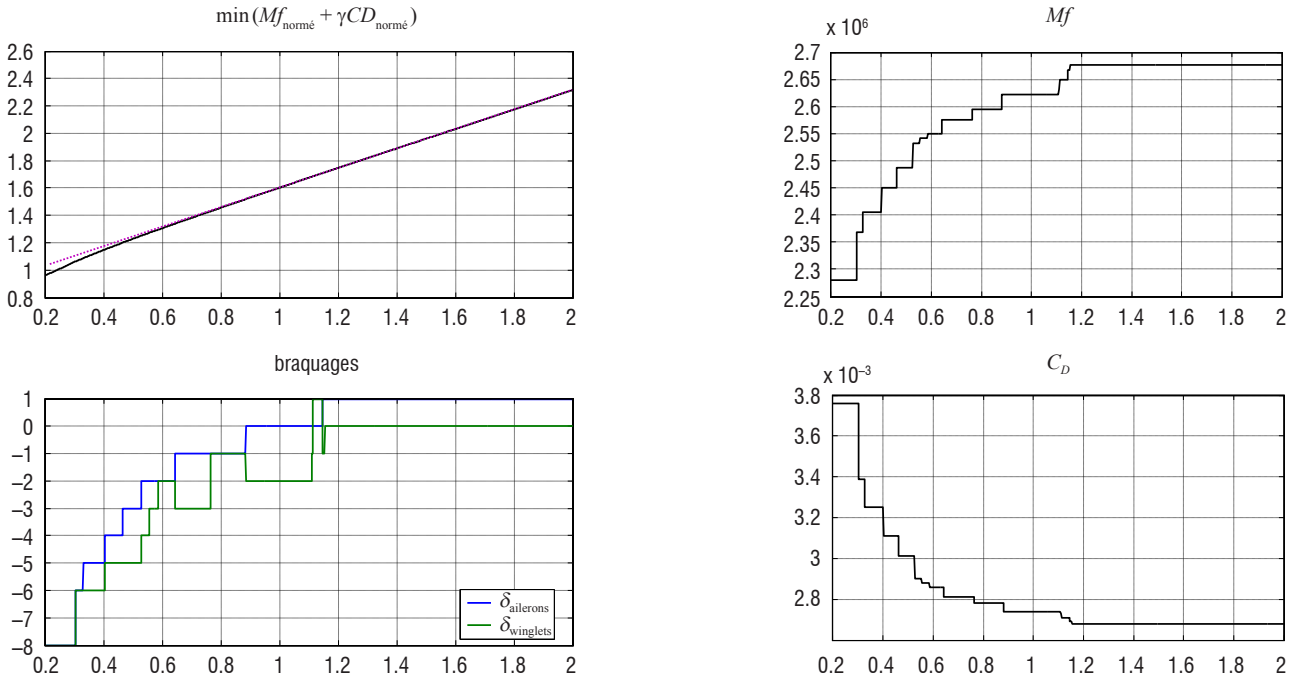

Figure 17 – Optimal objective function, bending moment, aileron and winglet flap deflection and drag with respect to the drag weighting coefficient γ in the objective function expression (bending moment + γ drag)

aero-structure optimization or for control-surface function optimization. The response surfaces of the bending moment, drag, sum of these and product of these have therefore been determined in a reasonable time for aileron and winglet flap deflections ranging from –8° to 8° (Figure 16). One can note that the minima of the drag and the quantities involving drag are reached for deflections close to 0 but not null. Furthermore, the curvature of the drag behavior with respect to the aileron deflection is higher than that with respect to the winglet flap deflection, thus showing a significantly stronger impact of the aileron on the drag than that of the winglet flap.

A preliminary study has been carried out to compute the optimal deflections of both the aileron and the winglet flap according to an objective function built from both the load (bending moment at the wing root) and the aerodynamic performance (drag) contributions:

$$\min\left[Mfx/Mfx_0 + \gamma\, C_D/C_{D0}\right]$$

In order to make the objective function coherent and thus make the bending moment and the drag coefficient dimensionless, the latter variables have been divided by reference values (Mfx_0 and C_{D0} matching the maximal values in the top sketches of Figure 16). Furthermore, the drag coefficient is deduced only from the Trefftz formulation, without any CFD result contribution. Only the induced drag is therefore considered for the optimization process. A weighting coefficient γ has been applied to the drag contribution, in order to investigate the influence of one contribution on the other. An optimization problem has thus been solved for values of this weighting coefficient ranging from 0.2 to 2. The optimal deflections of both the aileron and the winglet flap are plotted in Figure 17 – Optimal objective function, bending moment, aileron and winglet flap deflection and drag with respect to the drag weighting coefficient g in the objective function expression (bending moment + γ drag). The latter shows that the optimal deflection of the winglet flap is similar to that of the aileron for the entire range of γ. The winglet flap used in association with the aileron therefore has a significant efficiency for load alleviation, while having lower impact on the drag. Future works will be dedicated to finding the optimal aileron-winglet flap deflection configurations for several flight conditions, in order to assess the real gain in structure weight and fuel consumption.

Technological aspects

Additional work has been performed to ensure the feasibility of the trailing-edge-flap winglet concept. Nevertheless, the aim of the previous study was just to prove that it is possible to design a demonstrator using current technologies. In this context, we did not pay particular attention to certification requirements, as presented in [17] for the winglet adaptive trailing edge development carried out within the framework of the European project SARISTU. Aerodynamic calculations showed that the proposed control surface should have the following performances:

- Hinge moments: 67 mN, 13 mN and 28 mN at +10°, –10° and 0° flap deflection respectively.
- Maximal flapping frequency of 5 Hz.
- Ability to operate at cruise flight conditions, *i.e.*, Mach = 0.7 and an altitude of 35,000 ft (this flight altitude imposes an operating temperature of –55°C for the actuator).

Preliminary calculations showed that it was not possible to find actuators and a hinge geometry able to ensure the required hinge moments for flap deflections of +/–10° at 5 Hz. Consequently, the initial requirement regarding the flap amplitude has been reduced to +/–5°.

The first problem that arose was the implementation of a movable control surface of about 30% of chord at the trailing edge. Starting

from the initial finite-element mesh, the winglet spar ribs and skins have been redesigned to take into account a straight flap hinge (red line in Figure 18 left). The most suitable area to implement an actuator was the winglet root, where the available room is the widest (Figure 18 middle). These conditions lead to a slight modification of the initial finite-element mesh, as shown in Figure 18 right.

The second step has consisted in selecting an actuator satisfying all of the constraints (geometry, forces, operating temperature, dynamics and energy consumption). Taking into account the cruise aerodynamic conditions, a deflection ranging from –10° to 10° yields a maximal aerodynamic moment of 67 Nm. The actuator should be able to apply this moment with a moment arm measuring less than 42 mm, since it has to be located in a reduced volume. The most suitable actuator has to have the following characteristics: maximal effort of 10,000 N for a displacement amplitude of 20 mm. The dynamic operating speed has therefore been deduced from the required displacement and from the specified deflection amplitude and frequency. Owing to the cruise altitude, the actuator should also be able to operate at low temperatures of about –55°C. An electrical actuator seems to be the most suitable, but it also has to satisfy additional constraints, such as low energy consumption and the ability to use a power supply system compatible with that of the aircraft (voltage lower than 400 V). Some commercial actuators meet all of these specifications, as can be seen in [11]. It is important to note that only cruise conditions have been taken into account and other conditions such as "off-design" (take off, climb, descent, and landing) should also be considered to achieve the feasibility of the demonstrator. Unfortunately, this leads to greater loads requiring a specific actuator design to meet all certification requirements, as has been performed in [12].

The next step consisted in studying the implementation of the actuator and flap in the winglet. Figure 19 shows a planform view of the flap, the actuator location, the hinge axis and the kinematic connections. A more detailed view of the installation of the actuator in the winglet box and its connection with the flap is given in Figure 20. The initial finite-element model has therefore been modified to represent the morphing system as accurately as possible.

The additional mass of the actuator, connecting rods and ball joints is 13.18 kg and that of the flap is 2.925 kg. The flap spars and stiffeners are made of an aluminum alloy and the flap skin is made of the same composite material as that of the wing. Finite-element computations have also been performed based on the aerodynamic forces deduced from the specifications. A first static simulation was carried out applying pressure forces to the flap skin (Figure 21 left) and a second simulation was carried out applying forces deduced from the maximal effort of the actuator (9600 N) to the actuator fixation nodes (Figure 21 right). These simulations have shown a maximal displacement of 0.458 mm at the winglet and a maximal stress of about 21 Mpa, which are values lower than the admissible ones.

This technological work is obviously not sufficiently complete to manufacture a high TRL demonstrator, but was aimed solely at demonstrating the feasibility of the concept of the morphing trailing-edge winglet. It has indeed shown that a flap could be mounted on a winglet

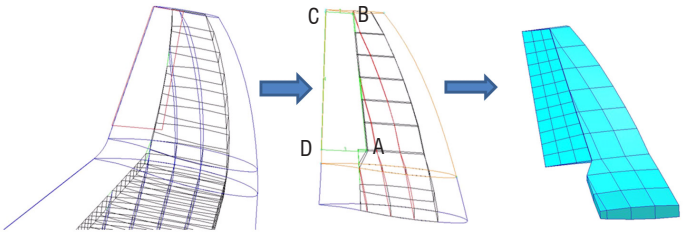

Figure 18 – New winglet box design and modified finite-element model

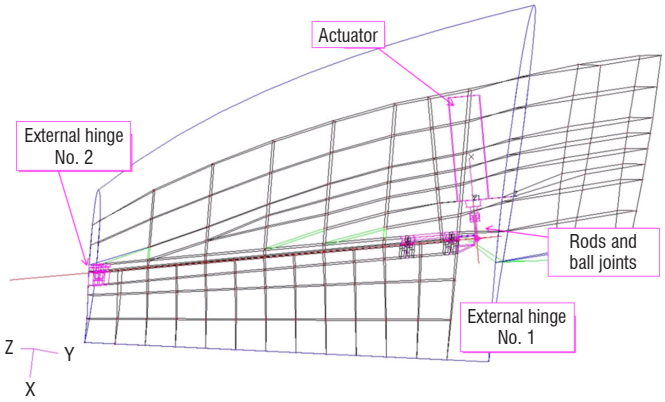

Figure 19 – Implementation of a flap and an actuation system in the winglet

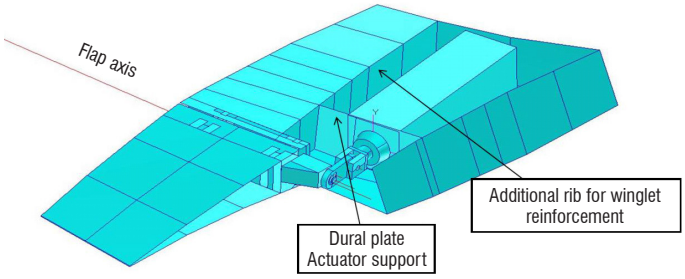

Figure 20 – Focus on the actuator and its installation in the central box

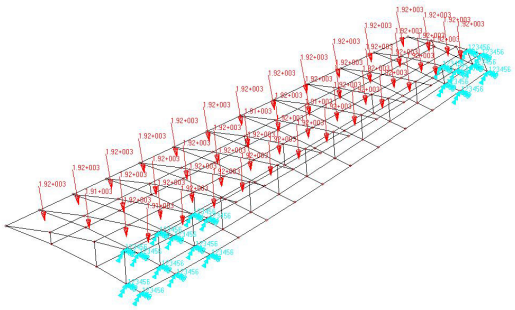

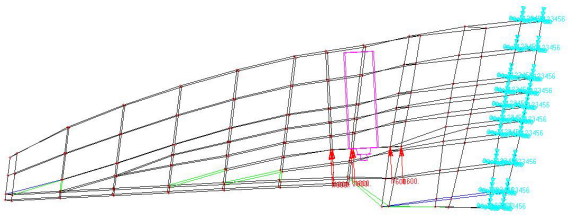

Figure 21 – Sizing static simulation boundary conditions and applied loads

using commercial actuators, even though no demonstrator has been built. Moreover, the problem of designing a skin covering the entire winglet allowing smooth flap deflections has not been addressed in this study. Furthermore, improvement could be envisaged in the case of a full scale winglet, by optimizing the actuator location to increase its travel and to improve its efficiency, and by optimizing the connecting rod angles to increase the moment arm.

Conclusions

One priority for the aeronautic community is now to significantly decrease the environmental footprint of aircraft. One possible way is to improve aerodynamic load control and alleviation, while improving, or at least not altering the aerodynamic performance, in order to decrease the structure weight. In this context, several morphing winglet concepts have been evaluated from the load control point of view.

The first step consisted in developing a numerical simulation tool able to accurately capture most physical phenomena, while remaining reasonable in terms of computational time. This software is based on coupling the publicly available static flight mechanics software AVL with an aeroelastic reduced model able to take into account the structure dynamics, structural deformations and unsteady aerodynamics. This reduced model is based on a state-space model built from a set of structure deformation modes and from a rational function approximation of aerodynamic forces, according to the Roger formulation. This state-space model has been validated by comparisons with CFD and high-fidelity coupling fluid-structure (CFD-CSM) for the aerodynamic conditions of interest (high subsonic flight). The coupled aeroelastic model is then able to assess the performance of a flexible free-free aircraft, which is trimmed for a specified maneuver. This performance can be seen from the aerodynamic (lift or drag), load control (bending or torsion moment, vertical effort) and aeroelastic (vertical displacement, twist variation, control surface efficiency) points of view. Furthermore, since the model is low-CPU-time-consuming, it can be used in an optimization process for control-surface design, as well as for designing a control surface driving strategy.

The second step consisted in the determination of a reference wing, which has to be the most representative of a real aircraft equipped with a winglet. Such a wing has been designed from the wing specifications and geometry of a regional aircraft determined within the EU project SARISTU [30] and from several sizing load cases (both symmetric and asymmetric maneuvers) extracted from the certification standard documents (CS 25). The aeroelastic stability has also been checked.

In a third step, four morphing winglet concepts were assessed in terms of aerodynamic performance and load control for subsonic-cruise-like conditions: flapping winglet (rotation of the winglet around the wing-tip chord axis), rotation of the whole winglet around its spanwise axis, torsional winglet (controllable torsion deformation) and a trailing edge control surface. The winglet with trailing edge flap was found to be the most efficient in terms of load control, in particular when used in conjunction with the aileron. This morphing concept indeed has significant efficiency, though less than that of the aileron, but has a weaker impact on drag.

The last step consisted in investigating the technological feasibility of such a morphing concept. This study did not lead to the building and testing of a demonstrator, as in the work by Wildschek *et al.* within the framework of the EU project SARISTU [30 Part III] [27], but it proved that the concept could be implemented in both a demonstrator and a real aircraft ■

References

[1] ACARE - *Strategic Research & Innovation Agenda (Volume 1)*. www.acare4europe.org/sites/acare4europe.org/files/attachment/acare-strategic-research-innovation-volume-1-v2.7-interactive-fin.pdf.

[2] E. ALBANO, W. RODDEN - *A Doublet-Lattice Method for Calculating Lift Distributions on Oscillating Surfaces in Subsonic Flow*. AIAA Journal 7(2), pp. 279-285, 1969.

[3] A. ALLEN, C. BREITSAMTER - *Investigation on an Active Winglet Influencing the Wake of a Large Transport Aircraft*. 25th International Congress of the Aeronautical Sciences ICAS2006, Hamburg, 3-8 September 2006.

[4] J. D. ANDERSON - *Fundamentals of Aerodynamics*. Mac Graw Hill, 2001.

[5] S. BARBARINO, O. BILGEN, R. M. AJAJ, M. I. FRISWELL, D. INMAN - *A Review of Morphing Aircraft*. J. Intel. Mat. Syst. Str. 22, 823-877, 2011.

[6] W. BRIX - *Subsonic Aircraft with Backswept Wings and Movable Wing Tip Winglets*. US patent no. US 6,345,790 B1, 12 February 2002.

[7] L. CAMBIER, S. HEIB, S. PLOT - *The ONERA elsA CFD Software: Input from Research and Feedback from Industry*. Mechanics & Industry 14(3) pp 159-174, doi: 10.1051/meca/2013056, 2013.

[8] I. CHOPRA - *Review of Sate of Art of Smart Structures and Integrated Systems*. AIAA Journal 40(11) 2145-2187, 2002.

[9] A. CONCILIO, I. DIMINO, L. LECCE, R. PECORA - *Morphing Wing Technologies Large Commercial Aircraft and Civil Helicopters*. 1st Edition, Elsevier, 19 October 2017.

[10] J. E. COOPER, I. CHEKKAL, R. C. M. CHEUNG, C. WALES, N. J. ALLEN, S. LAWSON, A. J. PEACE, R. COOK, P. STANDEN, S. D. HANCOCK, G. M. CAROSSA - *Design of a Morphing Wingtip*. AIAA Journal of Aircraft, Vol. 52 No 5, September 2015.

[11] DIAKONT - *Actionneurs electro-mécaniques (EMA) Séries DA*. SNT catalog.

[12] I. DIMINO, G. AMENDOLA, B. DI GIAMPAOLO, G. IANNACCONE, A. LERRO - *Preliminary Design of an Actuation System for a Morphing Winglet*. 8th International Conference on Mechanical and Aerospace Engineering (ICMAE), Prague, 2017.

[13] M. DRELA, H. YOUNGREN - *AVL*. http://web.mit.edu/drela/Public/web/avl/.

[14] M. GAZAIX, A. JOLLES, M. LAZAREFF - *The elsA Object-Oriented Computational Tool for Industrial Applications.* 23rd Congress of ICAS Toronto Canada, 8-13 September 2002.

[15] P. GIRODROUX-LAVIGNE - *Progress in Steady/Unsteady Fluid-Structure Coupling with Navier-Stokes Equations*. International Forum on Aeroelasticity and Structural Dynamics, Munich Germany, 28 June – 1 July 2005.

[16] P. GIRODROUX-LAVIGNE - *Recent Navier-Stokes Aeroelastic Simulations using the elsA Code for Aircraft Applications.* International Forum on Aeroelasticity and Structural Dynamics, Stockholm Sweden, 18-20 June 2007.

[17] C. HEINEN, A. WILDSCHEK, M. HERRING - *Design of a Winglet Control Device for Active Load Alleviation*. International Forum on Aeroelasticity and Structural Dynamics (IFASD), Bristol UK, 2013.

[18] S. J. MILLER - *Adaptive Wing Structures for Aeroelastic Drag Reduction and Loads Alleviation*. University of Manchester, PhD thesis, September 2010.

[19] R. PECORA, F. AMOROSO, G. AMENDOLA, A. CONCILIO - *Validation of a Smart Structural Concept for Wing-Flap Camber Morphing*. Smart Structures and Systems, Vol. 14 Issue 4, pp. 659-678, 2014.

[20] F. PETER, E. STUMPF, G. CAROSSA - *Morphing Value Assessment on Overall Aircraft Level (Chapter XI)*. Wolcken PC, Papadopoulos M (eds) Smart Intelligent Aircraft Structures (SARISTU) (Proceedings of the final project conference), Berlin, Heidelberg: Springer-Verlag, pp. 859-872, 2015.

[21] A. V. POPOV, T. L. GRIGORIE, R. M. BOTEZ, Y. MERBAKI - *Real Time Morphing Wing Optimization Validation Using Wind-tunnel Tests*. Journal of Aircraft 47(4), July 2010.

[22] K. L. ROGER - *Airplane Math Modeling Methods for Active Control Design.* CCP-228, AGARD, August 1977.

[23] M. M. K. V. SANKRITHI, J. B. FROMMER - *Controllable winglets*. US patent no US 2008/0308683 A1, 18th December 2008.

[24] S. H. TIFFANY, W. M. ADAMS Jr - *Nonlinear Programming Extensions to Rational Function Approximation Methods for Unsteady Aerodynamic Forces*. NASA-TP-2776, July 1988

[25] T. A. WEISSHAAR - *Morphing Aircraft Technology - New Shapes for Aircraft Design*. NATO meeting proceedings RTO-MP-AVT-141, 2006.

[26] A. WILDSCHEK, R. MAIER - *Winglet with Autonomously Actuated Tab*. Patent no EP 2233395 A1, 29 September 2010

[27] A. WILDSCHEK, S. STORM, M. HERRING, D. DREZGA, V. KORIAN, O. ROOCK - *Design, Optimization, Testing, Verification, and Validation of the Wingtip Active Trailing Edge.* "Smart Intelligent Structures (SARISTU)", pp. 219-255, Springer 2016.

[28] A. WILDSCHEK, S. STORM, J. KIRN - *Wingtip Active Trailing Edge for Loads Alleviation*. ECOMAS Congress 2016.

[29] R. T. WHITECOMB - *A design Approach and Selected Wind-tunnel Results at High subsonic Speeds for Wing-Tip Mounted Winglets*. NASA TN D-8260 July 1976.

[30] P. C. WOLCKEN, M. PAPADOPOULOS Editors - *Smart Intelligent Aircraft Structures (SARISTU) Proceedings of the Final Project Conference*. Springer.

AUTHORS

Cédric Liauzun graduated from the *Ecole Nationale Supérieure de Mécanique et d'Aérotechniques* (ENSMA) in 1996, and has about 20 years of experience as a member of the Numerical Aeroelasticity team at ONERA, where his activity is mainly devoted to the development of numerical simulation methods for aeroelasticity and fluid-structure coupling.

Dominique Le Bihan has been a Research and Test Engineer for the Aeroelasticity and Structural Dynamic Department, at ONERA, in Châtillon, France, since 1980. He was involved in technical support for wind tunnel test facilities and, a few years later, became active in linear control law design, mainly applied to the reduction of internal vibration and acoustics in aircraft and helicopters. He is currently involved in flutter and dynamic response reduction, and load alleviation on wind-tunnel mock-up and aircraft models. His current research interests include the dynamics of structures (modeling and identification), and fluid-structure coupling by mean of an aeroelastic state-space model and numerical aerodynamic tools.

Jean-Michel David graduated from the "*Ecole Nationale Supérieure de Mécanique de Nantes*" in 1981. He received a PhD in Acoustics from the "*Ecole Doctorale de Lyon*" in 2005. He worked for a long time as a research engineer in Acoustic Discretion and Vibroacoustics for ONERA's Structural Department in Chatillon, since 2009. He is now involved in aircraft and turbomachinery numerical aeroelasticity in the Aerodynamics, Aeroelasticity and Acoustics Department (DAAA), where his knowledge and experience in Structural Dynamics are strongly appreciated.

Didier Joly has been a Research and Test Engineer for the Material and Structural Department, ONERA-Lille, since 1981. He has worked on helicopter blade design for 20 years. His activity is now devoted to the study, design, and technological development of new blade and aircraft structure concepts.

Bernard Paluch graduated from engineering school in 1983, and has about 30 years of experience at ONERA in various fields, such as composite materials, numerical simulations and aircraft structural design. His main activity is now devoted to structural concept evaluation in association with Multi-Disciplinary Analysis and Optimization tools developed at ONERA for Hybrid Propulsion Aircraft, Blended Wing Body, and reusable space launchers.